Supramolecular Assembly Promotes the Electrocatalytic Reduction of Carbon Dioxide by Re(I) Bipyridine Catalysts at a Lower Overpotential

Charles W. Machan,[†] Steven A. Chabolla,[†] Jian Yin,[‡] Michael K. Gilson,*[,‡] F. Akif Tezcan,[†] and Clifford P. Kubiak*[,†]

[†]Department of Chemistry and Biochemistry, University of California-San Diego, 9500 Gilman Drive, La Jolla, California 92093-0358, United States

[‡]Skaggs School of Pharmacy and Pharmaceutical Sciences, University of California-San Diego, 9500 Gilman Drive, La Jolla, California 92093-0736, United States

Ⓢ Supporting Information

ABSTRACT: The addition of methyl acetamidomethyl groups at the 4,4′-positions of a 2,2′-bipyridyl ligand is found to enhance the rate of a bimolecular reduction mechanism of CO_2 by Re^I *fac*-tricarbonyl chloride complexes. Electrochemical studies, spectroelectrochemical measurements, and molecular dynamics simulations indicate that these methyl acetamidomethyl groups promote the formation of a hydrogen-bonded dimer. This supramolecular complex catalyzes the reductive disproportionation of CO_2 to CO and CO_3^{2-} at a lower overpotential (ca. 250 mV) than the corresponding single-site 2 e$^-$ reduction of CO_2 to CO and H_2O catalyzed by the corresponding model complex with a 4,4′-dimethyl-2,2′-bipyridyl ligand. These findings demonstrate that noncovalent self-assembly can modulate the catalytic properties of metal complexes by favoring alternate catalytic pathways.
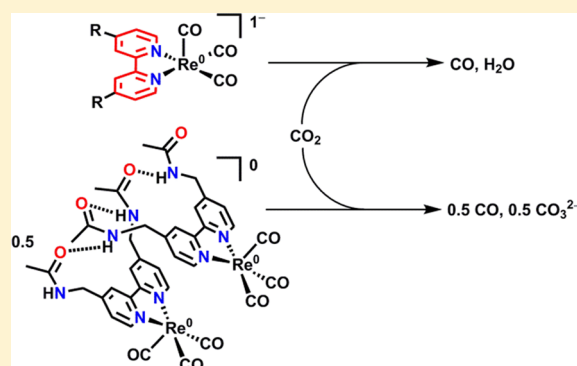
■ INTRODUCTION

Electrochemical reduction of CO_2 to liquid fuels is a promising way to achieve a carbon neutral energy cycle by connecting fuel production to combustion byproducts, especially when driven by solar, wind, or hydrogenated electricity.[1−6] One of the most extensively studied molecular catalysts for the electrochemical reduction of CO_2 is the Re^I(2,2′-bipyridyl)-based system, originally developed by Lehn and co-workers [2,2′-bipyridyl = bpy].[7] The Re^I(bpy) catalyst system has a high Faradaic efficiency for the generation of CO in the presence of weak acids.[8−10] The reaction catalyzed is a two-proton/two-electron (2 H$^+$/2 e$^-$) reduction of CO_2 to CO and H_2O, and the addition of weak acids increases the turnover frequencies (TOFs) significantly. This complex can also photocatalyze the reduction of CO_2 in the presence of a sacrificial reductant.[11]

While Re^I(bpy) molecular catalysts for the reduction of CO_2 can be highly active (TOF > 500 s^{-1}), selective for CO_2 reduction over H$^+$ reduction, and durable, they still do not approach the high kinetic and thermodynamic efficiencies (low overpotentials) of natural enzymes. Enzymes that catalyze the electrochemical reduction of CO_2 include the carbon monoxide dehydrogenases (CODHs) and formate dehydrogenases (FDHs).[12−14] These can achieve TOFs > 10,000 s^{-1} at overpotentials of <100 mV from $E^0(CO_2/CO)$ or $E^0([CO_2 + H^+]/HCO_2^-)$.[15,16] The Re^I(bpy) catalysts can achieve TOFs of

570 s^{-1} at an overpotential of ∼1 V from $E^0(CO_2/CO)$.[10] However, enzymes are far less chemically and physically robust and, therefore, require repair mechanisms to sustain catalysis.[17−19] In recent years, certain elements of natural enzymes have been successfully adopted to improve non-enzyme catalysts. These include the incorporation of proton relays into artificial hydrogenases[20−23] and iron tetraphenylporphyrin electrocatalysts for CO_2 reduction.[24]

We are investigating the possibility of further enhancing catalytic performance through the fabrication of hybrid structures that combine peptidic and organometallic components. This investigation takes its cue from biology, where enzymatic metalloproteins use dynamic channels to feed protons, electrons, and substrate to active sites in order to effect catalytic reactions at near thermodynamic potentials.[25−27] The Re^I(bpy) catalyst was selected for these studies for both its high activity and its ability to accept protons from a variety of sources.[8−10]

During our exploration of methods for catalyst incorporation into peptidic scaffolds, we synthesized a Re^I(bpy) catalyst with a bpy moiety modified with methyl acetamidomethyl substituents. This simple variant was unexpectedly found to

Scheme 1. Reduction Scheme for Re Bipyridine-Based Electrocatalysts[a]
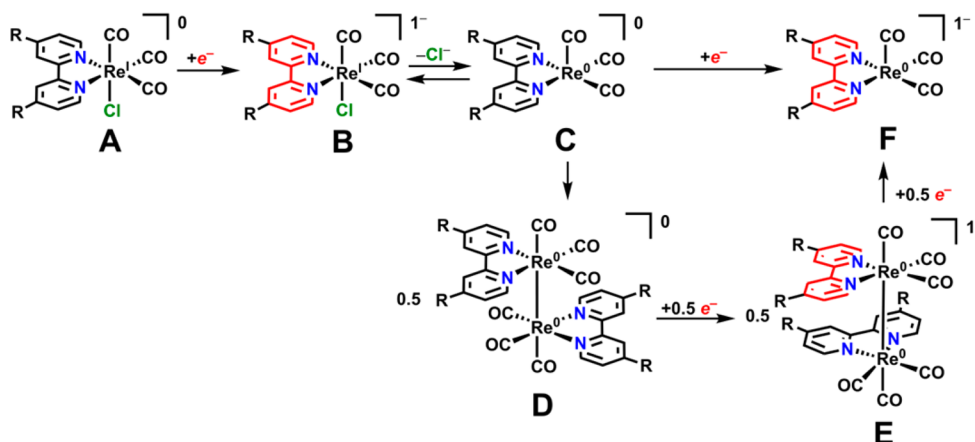
[a]Catalysts with non-interacting functional groups, i.e., R = Me, generally proceed from species **A** to **B** to **C** to **F** during electrocatalysis. A competing pathway through a metal–metal dimer is also shown.

Scheme 2. Proposed Mechanism for Electrocatalytic Reduction of CO_2 by Complexes of the Type $Re^0(bpy)(CO)_3$ Which Is Second Order in Catalyst and Generates CO_3^{2-}
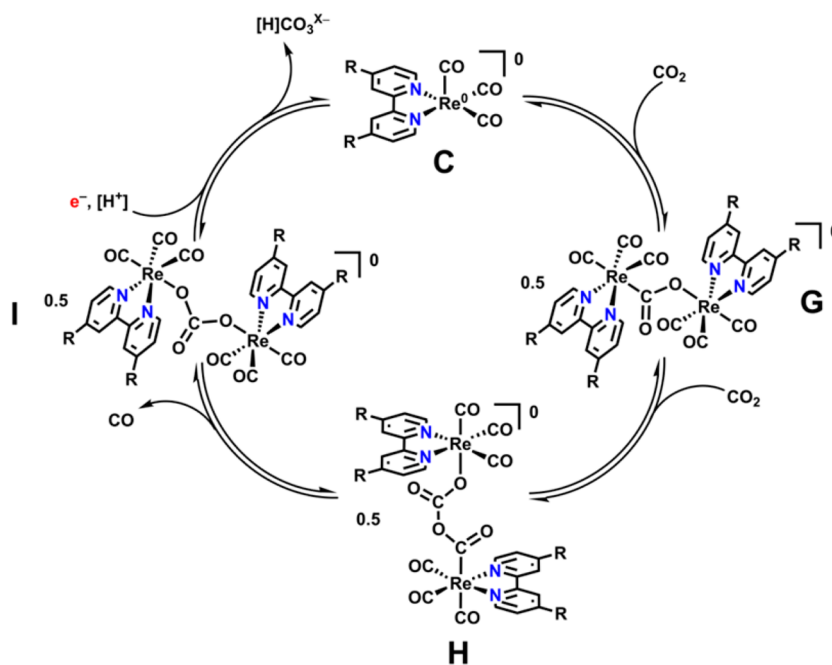

have electrochemical behavior strikingly different from that of previous $Re^I(bpy)$-based catalysts, under both N_2- and CO_2-saturation conditions. Here we describe how computational models, tested against electrochemical measurements and infrared spectroelectrochemistry (IR-SEC), indicate that the behavior of this catalyst results from a hydrogen-bond-mediated dimerization. This noncovalent dimerization process leads to an alternate catalytic mechanism for the reduction of CO_2, with a bimolecular 2 [Re(bpy)]/[1e⁻ + 1e⁻] process instead of a single-site [Re(bpy)]⁻/2e⁻ one, and leads to a change in the products of the reaction. As a prologue to the experimental and computational results, a summary of relevant background information regarding the unimolecular and bimolecular catalytic mechanisms of Re(bpy) catalysts is presented here.

Catalytic Mechanisms of Re(bpy)-Based Complexes. In order for a Re(bpy)-based complex to act as a catalyst, its parent state, **A**, must be reduced by one electron, to form the anionic species **B**, $[Re^I(bpy^\bullet)(CO)_3Cl]^-$ (Scheme 1). This complex loses chloride to form **C**, $[Re^0(bpy)(CO)_3]$, which can be reduced by an additional electron equivalent to form **F**, $[Re^0(bpy^\bullet)(CO)_3]^-$, which is catalytically active for the reduction of CO_2. In certain cases, it is possible for **C** to dimerize by forming a metal–metal bond. The resulting dimer **D**, $[Re^0(bpy)(CO)_3]_2$, may be reduced by one electron to form the anionic dimer **E**, $[Re^0(bpy)(CO)_3]_2^-$, before the metal–metal bond is cleaved by a second reduction to generate **F**.[28] The oxidation state assignment of **F** has been validated by extended X-ray absorption fine structure (EXAFS) studies, chemical reductions, computation, and infrared spectroelectrochemistry (IR-SEC).[28–33] This electronic structure appears to lead to lower kinetic barriers for the binding and reduction of CO_2/H^+ over H^+.[32]

A bimolecular mechanism has also previously been proposed for Re(bpy)-based complexes (Scheme 2).[34–36] Sullivan et al.

Scheme 3. Synthetic Scheme for Complex 1[a]
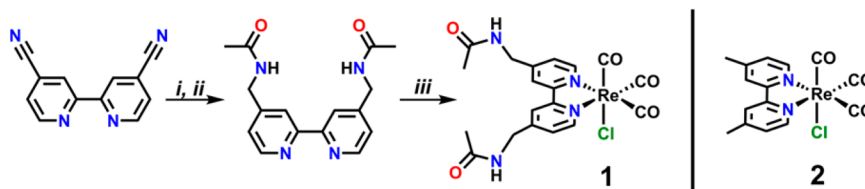
[a](i) Pd/C, H₂ (20 atm), ethanol/tetrahydrofuran (4:1), 50 °C, overnight; (ii) 2.1 equiv acetic anhydride, 2.1 equiv triethylamine, CH₂Cl₂; (iii) 1 equiv rhenium(I) pentacarbonyl chloride [Re(CO)₅Cl], toluene, reflux, 3 h.

observed that bulk electrolysis of solutions containing Re^I(bpy)(CO)$_3$Cl at the first observed reduction potential catalyzed the reductive disproportionation of 2 equiv of CO$_2$ to CO and CO$_3{}^{2-}$.[34] It was proposed that 2 equiv of the singly reduced species **C** would react to form a bridging CO$_2$ adduct, **G**, before the insertion of a second equivalent of CO$_2$ and that subsequent reductive disproportionation would complete the cycle.[35] Later computational work indicated that the CO$_2$ insertion product **H** and the product of subsequent CO loss **I** were likely intermediates.[36]

It is worth noting that the existence of two electrocatalytic pathways involving uni- or bimolecular mechanisms is reminiscent of the H$_2$-evolving cobaloxime electrocatalysts.[37−39] Unlike the case of cobaloxime, however, the alternate pathways of the Re(bpy) electrocatalysts differentiate in the observed products; the unimolecular mechanism generates CO and H$_2$O, whereas the bimolecular mechanism catalyzes the reductive disproportionation of 2 equiv of CO$_2$ to CO and CO$_3{}^{2-}$. In view of the primary mechanistic possibilities for this class of Re(bpy) electrocatalysts, we move next to a discussion of the results.

RESULTS

Synthesis. Re((4,4′-bis(methyl acetamidomethyl)-2,2′-bipyridine)(CO)$_3$Cl, **1**, was synthesized in three steps from commercially available precursors (4,4′-bis(methyl acetamidomethyl)-2,2′-bipyridine = dac, Scheme 3)[40] and characterized by NMR spectroscopy, microanalysis, and ESI-MS. Single crystals suitable for X-ray diffraction studies were grown from a supersaturated solution of **1** in methanol (CH$_3$OH) at −20 °C, which confirmed the proposed molecular structure (Figure 1).
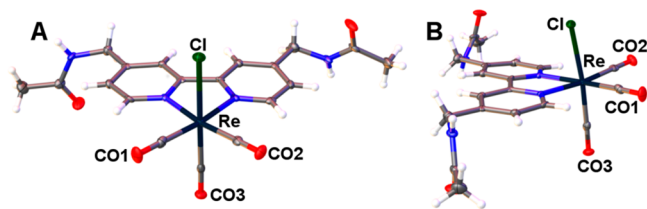

Figure 1. Single-crystal X-ray crystallographically determined molecular structure of **1**, with front (A) and side (B) views. Occluded MeOH molecule omitted for clarity, C = gray, N = blue, Re = navy, O = red, H = white, Cl = green; thermal ellipsoids shown at 50%.

Complex **1** has a six-coordinate Re(I) center with a *fac*-tricarbonyl arrangement. A fully chelated bipyridine ring occupies the two remaining equatorial positions, with an axial Cl⁻ ligand. Model complex **2**, Re^I(4,4′-dimethyl-2,2′-bipyridyl)-(CO)$_3$Cl [4,4′-dimethyl-2,2′-bipyridyl = dmb], was prepared according to literature procedures.[41]

Initial Electrochemical Studies of 1. In order to characterize the redox and electrocatalytic behavior of **1** in comparison to the model complex **2**, cyclic voltammograms (CVs) were taken under N$_2$- and CO$_2$-saturation conditions in acetonitrile (MeCN) solutions (0.1 M tetrabutylammonium hexafluorophosphate, TBAPF$_6$). The influence of the methyl acetamidomethyl groups on the electrochemical behavior of complex **1** is evident by cyclic voltammetry under N$_2$ atmosphere, as four redox processes were observed in a potential range where the model compound **2** exhibits two features (Figure 2A).[8,30,32] Starting from resting potential, an irreversible redox feature is observed at −1.77 V, a reversible one at −1.88 V, a quasi-reversible one at −2.14 V, and a final irreversible one at −2.34 V (versus Fc/Fc+). In comparison, complex **2** exhibits a reversible feature at −1.85 V and an irreversible one at −2.20 V (vs Fc/Fc+). Complex **1** also has an irreversible oxidation feature on the return sweep at −0.50 V vs Fc/Fc+. No corresponding oxidation feature is observed on the return sweep for **2**.

When the solution with **1** was sparged with CO$_2$ to saturation (∼0.28 M), an increase in current at the first reduction potential was observed with a peak at −1.98 V vs Fc/Fc+ (Figure 2B). For the model compound **2**, this increase under CO$_2$ atmosphere comes at the second redox potential.[8] The addition of 2,2,2-trifluoroethanol (TFE) as a proton source to the solution containing **1** caused a further increase in current under CO$_2$-saturation conditions, consistent with a proton-dependent catalytic reaction (Figure S1). Upon returning to N$_2$ saturation, no increase in current at any of the four features was observed as compared to the voltammograms of **1** taken prior to the addition of TFE. Electrochemical experiments with the dac ligand, validated by computational investigations, indicated that the methyl acetamidomethyl groups were not engaging in redox reactions on their own. Additionally, no reductive redox features were observed for control molecules containing methyl acetamidomethyl moieties. Probing the behavior of **1** in solvents with varying dielectric constants in conjunction with computational modeling indicated that the new behavior of **1** relative to model complex **2** did not originate from through-space dipole effects on the Re metal center on the bpy ligand. Specifically, the observed redox behavior could not be correlated with any trend in the dielectric constant. In summary, the observed electrochemical responses of **1** under N$_2$ and CO$_2$ saturation were not consistent with the well-established electrocatalytic mechanism for the unimolecular two-electron reduction of CO$_2$ to CO and H$_2$O by Re(bpy) complexes and were not readily explained by potential unimolecular mechanisms.

We conjectured that the amide moieties of **1** might be driving dimerization in an MeCN solution, which, although moderately polar, is a poor hydrogen-bond donor and acceptor
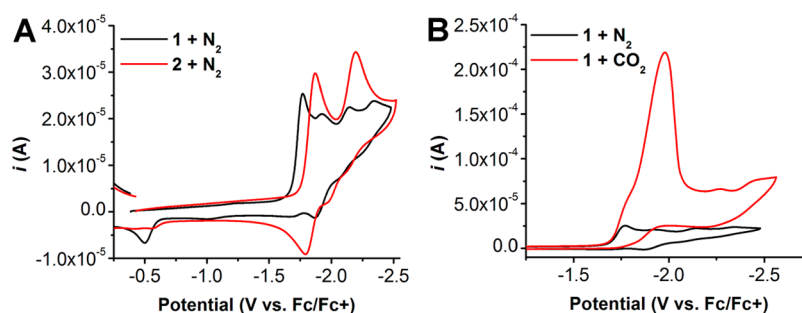
Figure 2. CVs showing the redox behavior of **1** and **2** at negative potentials (A) and **1** under CO_2-saturation conditions at negative potentials (B). Single compartment cell with GC WE, Pt wire CE, Ag/AgCl pseudo-RE (behind Vycor tip); 100 mV/s, 1 mM analyte, 0.1 M TBAPF$_6$/MeCN; referenced to internal Fc standard.

and, therefore, would not strongly compete against the formation of solute—solute hydrogen bonds. We therefore carried out additional electrochemical studies in *N,N*-dimethylformamide (*N,N*-DMF), which disrupts hydrogen bonding and has a similar dielectric constant to MeCN.[42]

CVs of **1** taken in *N,N*-DMF (1 mM in 0.1 M TBAPF$_6$/*N,N*-DMF) exhibited only two redox features: a reversible wave at −1.76 V and an irreversible wave at −2.13 V vs Fc/Fc+ (Figure 3). These redox features observed for **1** in *N,N*-DMF are
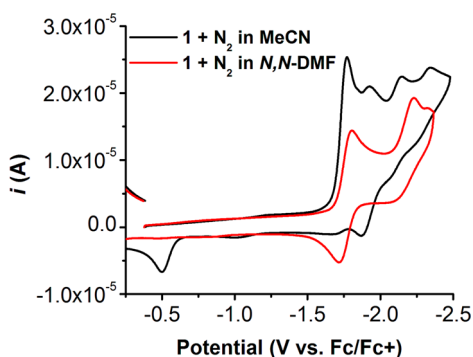

Figure 3. CVs comparing the redox behavior of **1** in *N,N*-DMF and MeCN at negative potentials. Conditions: 1 mM, 100 mV/s, 0.1 M TBAPF$_6$/MeCN (black), and 0.1 M TBAPF$_6$/*N,N*-DMF (red); GC WE, Pt wire CE, Ag/AgCl RE behind Vycor tip; referenced to internal Fc standard.

consistent with two consecutive single electron reductive processes similar to what is observed for the model complex **2** in both MeCN (Figure 2A) and *N,N*-DMF. Indeed, CVs of **2** taken under identical conditions showed a reversible wave at −1.84 V and an irreversible wave at −2.16 V vs Fc/Fc+ (Figure S2). Notably, no irreversible oxidation at −0.50 V vs Fc/Fc+ is observed on the return sweep for **1** under these conditions. Voltammograms of **1** and **2** under CO_2 atmosphere both showed an increase in current at the second redox feature in *N,N*-DMF (Figure S3). These results supported the conjecture that hydrogen-bond-driven interactions are playing a role in the electrochemical behavior of **1** in MeCN. We therefore examined this possibility further by using infrared spectroelectrochemistry (IR-SEC) and computational methods, as detailed in the following subsections.

IR-SEC Under N$_2$ Atmosphere. IR-SEC is a valuable technique for examining the behavior of electroactive species at applied potential and has been used with particular success in studying the mechanism of reduction and catalytic behavior of Re(bpy)-type electrocatalysts.[41,43−47] The method used in our

experiments is Fourier transform infrared reflectance spectroscopy (FTIR).[41,45] In these experiments a thin-layer of solution containing analyte is sealed between an IR-transparent CaF$_2$ window and a working electrode polished to a mirror finish within concentric reference and counter electrode rings. The contents of the resultant small-scale bulk electrolysis cell can be characterized with FTIR by directing the source laser to the reflective working electrode and through the sample before passing to the detector. When a potentiostat is used, changes in the observable IR bands can be monitored as a function of potential and time. In this manner the behavior observed by CV can be correlated to relevant species in solution for all accessible redox states. This makes IR-SEC an ideal tool to identify the products of electron transfer in solution.

IR-SEC of **1** in 0.1 M TBAPF$_6$/MeCN under N$_2$-saturation conditions revealed several important differences between it and previously published Re(bpy)-based catalysts (Figure 4).[41,43−47] For complex **1** [Re^I(dac)(CO)$_3$Cl], the loss of
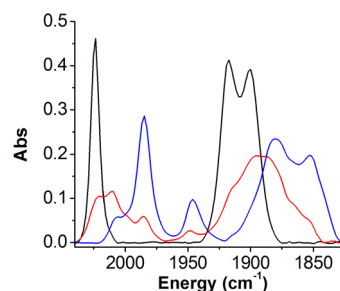

Figure 4. Selected spectra from IR-SEC studies of **1** showing that when the IR-SEC cell with complex [Re^I(dac)(CO)$_3$Cl] (black) is taken to the first reduction potential, the IR exhibits bands consistent with [Re^I(dac•)(CO)$_3$Cl]$^−$, [Re^0(dac)(CO)$_3$], and [Re^0(dac)(CO)$_3$]$_2$ (red). If the cell is held at this potential, the system equilibrates to the dimer [Re^0(dac)(CO)$_3$]$_2$ (blue). Single compartment cell with Pt WE, Pt wire CE, Ag pseudo-RE, 0.1 M TBAPF$_6$/MeCN.

chloride and the formation of a metal—metal bond after the initial reduction are quite rapid. When the IR-SEC cell is set to the first reduction potential, a species assigned to [Re^I(dac•)-(CO)$_3$Cl]$^−$ (2009, 1895, and 1886 cm^{-1}) is immediately observed, as is the product of chloride dissociation [Re^0(dac)-(CO)$_3$] (1998, 1875, and 1867 cm^{-1}). Before the complete disappearance of these three species, bands consistent with a metal—metal bound dimer [Re^0(dac)(CO)$_3$]$_2$ are also observed (1984, 1942, 1875, 1865, and 1842 cm^{-1}). The system eventually equilibrates almost entirely to the dimer at this potential. The formation of a Re^0−Re^0 dimer is known to
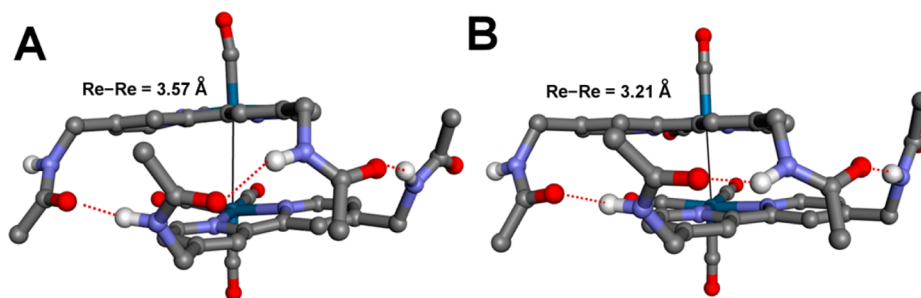
Figure 5. (A) The representative structure of the hydrogen-bonded dimer species from MD simulations in explicit MeCN. (B) The refined representative structure of $[Re^0(dac)(CO)_3]_2$ from DFT calculations. Hydrogen atoms not involved in hydrogen-bonding interactions and explicit MeCN molecules are omitted for clarity.

represent a competing pathway during the reduction of Re(bpy) complexes.[28] The formation of the metal–metal dimer raises the potential required for CO_2 reduction: following the formation of a Re^0–Re^0 bond, two reduction processes are required to cleave the Re–Re bond and generate a catalytically active species.

The methyl acetamidomethyl groups are also IR active, and the introduction of charge affects the amide modes. As the parent complex is reduced, the appearance of $[Re^0(dac)(CO)_3]$ and $[Re^0(dac)(CO)_3]_2$ accompanies a shift in the carbonyl stretch associated with the acetamidomethyl carbonyl group (Figure S4). The band of the parent compound is observed at 1685 cm^{-1}, which disappears and is replaced by two new broad bands at 1675 and 1668 cm^{-1}. This shift to lower frequencies is consistent with a hydrogen-bonding interaction and hence with the formation of a hydrogen-bonded dimer.[48,49] These results also indicate that the formation of a metal–metal bond is greatly accelerated for complex **1** and that hydrogen bonding played a role during the reduction of **1** and the formation of the metal–metal bond.

Computational Modeling of Hydrogen Bonding and Metal Dimerization. Computational methods were employed to model the hydrogen-bonding interactions in the observed redox behavior of **1**. Specifically, we examined the behavior of $[Re^0(dac)(CO)_3]$ in order to understand the mechanism behind the acceleration of metal–metal bond formation. Molecular dynamics (MD) simulations of two molecules of $[Re^0(dac)(CO)_3]$ in explicit MeCN led to the rapid (sub ns) formation of a stable hydrogen-bonded dimer, where the two monomers are held together by interlacing of the amide moieties to form a chain of intermolecular hydrogen bonds (Figure 5A). This outcome was observed for starting configurations in which the two $[Re^0(dac)(CO)_3]$ monomers were already stacked together and also for other starting configurations, including ones in which the monomers were initially positioned side-by-side. Once the dimer had formed, the monomers remained locked together for the rest of the simulation (50–100 ns), with only occasional fluctuations in the hydrogen-bond count. Matched simulations in *N,N*-DMF did not yield a stable dimer; instead, the two monomers rapidly drifted apart. The formation of a stable dimer structure in MeCN but not *N,N*-DMF is consistent with the observation that CVs of **1** taken in *N,N*-DMF did not show the same response as those taken in MeCN and with the expectation that the hydrogen-bonded dimers may be disrupted by competition with *N,N*-DMF for the hydrogen-bonding methyl acetamidomethyl groups.

In the representative dimer structure obtained from MD simulation (Figure 5A), all four methyl acetamidomethyl substituents are connected by a chain of three hydrogen bonds. This configuration placed the two Re atoms a distance of 3.57 Å apart. Refinement of this structure with density functional theory (DFT) in MeCN solvent led to minor structural adjustments (Figure 5B), except for a significant decrease of the Re–Re distance to 3.21 Å, consistent with the formation of a Re–Re bond. The computed Re–Re bond length of this dimer is similar to previously reported Re–Re bond lengths (3.0791(13) Å).[28] As noted above, the formation of a Re^0–Re^0 dimer species was observed experimentally by IR-SEC, consistent with these results. As a control, we ran similar MD simulations using explicit MeCN solvent with 2 equiv of $[Re^0(bpy)(CO)_3]$ to look for the possible formation of a stable neutral dimer. No stable dimers were observed, which we attribute to the absence of the hydrogen-bonding interactions in the case of $[Re^0(dac)(CO)_3]$. It should also be noted that the MD force field does not include terms that could lead to Re–Re bonding.

In order to examine the reduction mechanism of dimer $[Re^0(dac)(CO)_3]_2$, we used DFT methods, with implicit MeCN to optimize the structure of the one-electron reduced dimer species $[Re^0(dac^\bullet)(CO)_3]_2{}^-$, starting from the computationally determined structure of $[Re^0(dac)(CO)_3]_2$. The resulting structure of $[Re^0(dac^\bullet)(CO)_3]_2{}^-$ is almost identical to that of $[Re^0(dac)(CO)_3]_2$, with a root-mean-square deviation (RMSD) value of 0.09 Å and Re–Re distance of 3.22 Å. Attempts to obtain a converged structure by the addition of an electron to the singly reduced dimer species $[Re^0(dac^\bullet)(CO)_3]_2{}^-$ were unsuccessful. This result parallels the experimental observation that the addition of *two* electrons to Re^0–Re^0 dimer species of this type results in the cleavage of the metal–metal bond and the destabilization of the dimer configuration.[28] Optimization of the model compound $[Re^0(bpy)(CO)_3]_2$, starting with crystallographically determined coordinates (Re–Re distance ~3.08 Å), yielded little conformational shift and a Re–Re distance of 3.24 Å, Figure S5.[28] Previously reported DFT calculations also showed a slight overestimation of the Re–Re bond length.[50] MP2 calculations in the gas phase from the same study were found to be in better agreement with the crystallographic data. The size of the systems studied here made the computational cost of such calculations prohibitive, however.

Electrochemical Studies of Hydrogen Bonding and Metal Dimerization. To probe the mechanistic aspects of hydrogen-bonding interactions in the reduced complex, a series of electrochemical studies were undertaken with varying scan
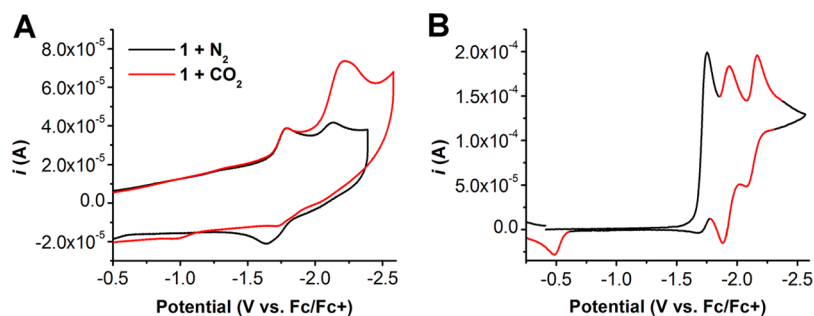
Figure 6. CVs showing the redox behavior of **1** at negative potentials at 0.1 mM (A) and 10 mM (B) concentrations. Single compartment cell with GC WE, Pt wire CE, Ag/AgCl pseudo-RE (behind Vycor tip), 0.1 M TBAPF$_6$/MeCN; A: 0.1 mM **1**, 1600 mV/s; B: 10 mM **1**, 100 mV/s, red indicates redox responses consistent with dimer formation; referenced to internal Fc standard.

rates and catalyst concentrations to probe the mechanism and kinetics of the metal−metal dimerization pathway for catalyst **1**. Variable scan rate experiments with **1** (1 mM in 0.1 M TBAPF$_6$/MeCN) under N$_2$-saturation conditions showed that the four observable features have different dependences on scan rate (Figure S6); in particular, at high scan rates, only two redox features predominate (Figure S7). Redox features with different dependences on scan rate are the result of chemical reaction steps following electrochemical steps, such as the dimerization or dissociation observed by IR-SEC and examined computationally above.

Under CO$_2$-saturation conditions, the peak catalytic current (i_{cat}) dependence on scan rate also shifted to more negative potentials with increasing scan rate (Figure S8). This behavior indicates that the catalyst is not operating at steady-state under these conditions and may also experience a shift in the predominant mechanism of CO$_2$ reduction. CVs of **1** at low concentrations (0.1 mM in 0.1 M TBAPF$_6$/MeCN) show the shift from four redox features at much slower scan rates (scan rates above 200 mV/s) than at 1 mM, which is indicative of a concentration-dependent component of the chemical steps following the initial reduction (Figures 7A and S9). At higher concentrations of **1** (10 mM in 0.1 M TBAPF$_6$/MeCN) only the first three redox features were observed (Figure 6B). The final redox feature observed at 1 mM concentrations of **1** disappeared entirely, indicating that the species represented by this redox feature is not favored at these concentrations.

Based on these results and the computationally determined structures, we reasoned that catalyst **1** may form a Re^0−Re^0 dimer on the CV time scale. This was confirmed by independent preparation of the Re^0−Re^0 dimer from **1** by bulk electrolysis at the first reduction potential.[51,52] Characterization of this dimer by cyclic voltammetry showed a reversible wave at −1.90 V and a quasi-reversible wave at −2.12 V vs Fc/Fc+, in good agreement with the second and third redox features observed for **1** (Figure S10, IR stretches: 1982, 1945, 1883, and 1847 cm^{-1}). The diffusion coefficient of the dimer was determined to be 7.82×10^{-6} cm^2/s (compared to 1.14×10^{-5} cm^2/s for **1**) by RDE methods, consistent with a more slowly diffusing electroactive species.[8,28] This electrolytically prepared metal−metal dimer exhibited an increase of current with CO$_2$ saturation at the second reduction potential, consistent with previous characterization of a Re^0−Re^0 dimer (Figure S10).[28] These results support the conclusion that the relevant active state of **1** forms before metal−metal bond formation. Computational results, above, indicate that a hydrogen-bonded dimer could form en route to a metal−metal bonded dimer, so that the unusual redox behavior of **1**

observed under CO$_2$-saturation conditions could result from an enhancement of the bimolecular reduction mechanism.

Electrochemical Experiments to Elucidate a Bimolecular Mechanism. As we have shown, a hydrogen-bonded dimer exists in the reduction mechanism of **1** in MeCN solution. In addition to this, catalytic current under CO$_2$-saturation conditions ensues from this dimeric species, before the formation of a metal−metal bond. Inasmuch as the hydrogen-bonded dimer is constructed from two monomers, this leads to the expectation that the overall rate of catalysis (as measured by current response), should have a second-order dependence on Re concentration. Indeed, the catalytic response was second order with increasing catalyst concentration between 0.1 and 6 mM (Figure S11). After 6 mM, increasing catalyst concentrations showed a linear response, which is indicative of saturation and the absence of a diffusion controlled mechanism. Consistent with this interpretation, the peak reductive current under CO$_2$ atmosphere catalyst concentrations above 6 mM shifted to more negative potentials, indicating a predominantly unimolecular mechanism (Figure S12). Establishing TOF under these conditions is difficult given the side phenomena occurring during the course of catalysis, but if the hydrogen-bonded dimer is treated as a first-order catalyst, a theoretical maximum rate for the reaction can be determined.[53] If the slowest step of the reaction is the hydrogen-bonded dimer reacting with CO$_2$, the peak catalytic current achieved (i_{cat}) represents the slowest reaction rate. When these considerations are applied to the following equation:[54,55]

$$\text{TOF} = k_{cat}[\text{Q}] = \frac{F\nu n_p^3}{RT}\left(\frac{0.4463}{n_{cat}}\right)^2\left(\frac{i_{cat}}{i_p}\right)^2$$

where R is the universal gas constant, T is the temperature, n_p is the number of electrons in the reversible non-catalytic reaction, n_{cat} is the number of electrons required for CO$_2$ reduction to CO, i_p is the peak current in the absence of CO$_2$, and ν is the scan rate, the *maximum* theoretical TOF is 19 s^{-1} under CO$_2$-saturation conditions and 57 s^{-1} with added TFE (0.795 M).

Computational Modeling of the CO$_2$ Bridged Dimer. Since these results were indicative of the previously discussed bimolecular mechanism of Re(bpy) complexes (Scheme 2), we reasoned that a bimetallic bridging CO$_2$ adduct stabilized by hydrogen bonds similar to **G** would be a catalytic intermediate.[34−36] Using DFT methods, such a complex was examined by the gas-phase optimization of 2 equiv of [Re^0(dac)(CO)$_3$] with 1 equiv of CO$_2$. The minimized structure consisted of an asymmetrically bound CO$_2$ bridging

two Re centers and exhibited hydrogen-bonding distances between the methyl acetamidomethyl moieties (Figure 7). The
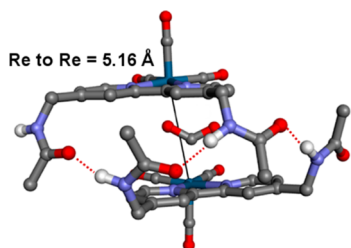

Figure 7. Converged structure of a bridging CO_2 adduct of type **G**, an expected intermediate in the catalytic cycle. The CO_2 molecule is asymmetrically bound to the two Re centers. Hydrogen atoms not involved in hydrogen-bonding interactions are omitted for clarity.

calculated bond lengths for the Re−O and Re−C bonds involving the CO_2 molecule, where insertion of a second equivalent of CO_2 would be expected to occur, are 2.16 and 2.24 Å, respectively. Facile insertion of a second CO_2 equivalent into these bonds would be a prerequisite for the increased current response observed by CV for complex **1** at the second reduction potential.

IR-SEC Under Catalytic Conditions to Determine Co-Product. Additional IR-SEC experiments under catalytic conditions revealed important information about some of the mechanistic aspects of this system. In a sample experiment, the cell was charged with **1** (3.6 mM), sparged briefly with $^{12}CO_2$, and set to the potential of the first reduction observed by cyclic voltammetry while sequential IR spectra were obtained. Interestingly, instead of observing a band consistent with H_2O (~1630 cm^{-1}), a possible product of the two-electron reduction of CO_2, two strong bands are observed to grow in at 1677 and 1648 cm^{-1}, consistent with CO_3^{2-} formation (Figure 8). As would be expected for a disproportionation reaction, a band also grows in at 2137 cm^{-1} corresponding to free CO in solution. Repeating these experiments with $^{13}CO_2$ showed a shift in all these bands, consistent with isotopic labeling. Indeed, free ^{13}CO is observed at 2090 cm^{-1} and $^{13}CO_3^{2-}$ 1632 and 1594 cm^{-1}, reflecting 38−47 cm^{-1} shifts, which is indicative of ^{13}C incorporation (ideal shift 45 cm^{-1} based on harmonic oscillator model).[56] After this experiment is run under $^{12}CO_2$ and returned to resting potential, the parent compound **1**

shows bands which are comparable to the starting material at 2020, 1913, and 1892 cm^{-1} (the high-frequency band observed at 2037 cm^{-1} corresponds to substitution of chloride by MeCN to form a solvent adduct). Interestingly, returning to resting potential after running the same experiment with $^{13}CO_2$ reveals that these bands have been replaced with stretches at 1997 and 1896 cm^{-1}, consistent with a ^{13}CO solvento adduct $[Re^I(dac)-(^{13}CO)_3(MeCN)]$, and bands at 1977 and 1871 cm^{-1}, indicative of isotopic labeling of the starting complex (Figure 8B). These experiments also show that the reaction catalyzed is the reductive disproportionation of CO_2 to CO and CO_3^{2-}, which is consistent with a bimolecular process.

Bulk Electrolysis Experiments to Determine Catalytic Efficiency. Bulk electrolysis experiments were combined with GC-MS to evaluate the efficiency of CO generation by **1** and **2** (1 mM in 0.1 M TBAPF$_6$; Table S1). At the first reduction wave, **1** generated CO with 56 ± 9% efficiency, which increased to 73 ± 7% with added TFE (0.5 M). The analogous experiments with **2** showed 46 ± 11% and 65 ± 16% (with 0.5 M TFE) efficiencies, respectively, at the first reduction. When these experiments were repeated at potentials more negative than the second reduction of **2**, the efficiency observed for **1** did not improve (54 ± 8%) but did for **2** (90 ± 5%), consistent with literature reports.[34] Control experiments under the originally reported conditions for this catalyst (10% H_2O in *N,N*-DMF) showed similar efficiencies for **1** (95 ± 9%) and **2** (95 ± 8%).[7]

■ SUMMARY AND CONCLUSIONS

At this point, it is helpful to review the electrochemical results that show four waves in the CVs of **1** in MeCN, and not *N,N*-DMF, and to interpret those results with the benefit of computational modeling and additional experiments. The four processes observed for **1** are at −1.77 V, −1.88 V, −2.14 V, and −2.34 V vs Fc/Fc +. The first two processes correspond to the reductions of hydrogen-bonded dimers ($[\mathbf{1A}\cdots\mathbf{1A}]$):
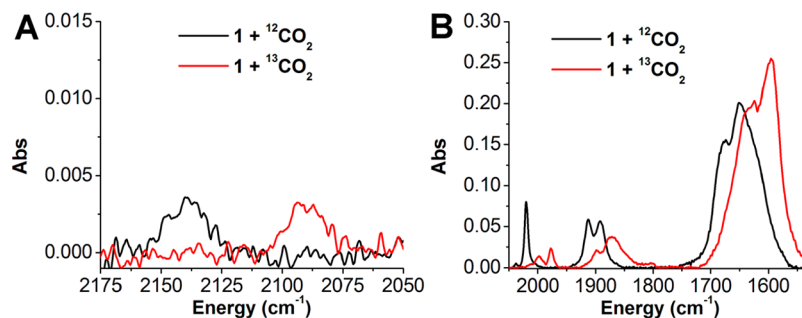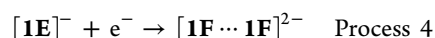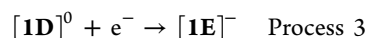
$$[\mathbf{1A}\cdots\mathbf{1A}] + e^- \rightarrow [\mathbf{1C}\cdots\mathbf{1A}] \quad \text{Process 1}$$

$$[\mathbf{1C}\cdots\mathbf{1A}] + e^- \rightarrow [\mathbf{1C}\cdots\mathbf{1C}]^0 \quad \text{Process 2} \quad ([\mathbf{1C}\cdots\mathbf{1C}]^0 \rightarrow [\mathbf{1D}]^0)$$

$$[\mathbf{1D}]^0 + e^- \rightarrow [\mathbf{1E}]^- \quad \text{Process 3}$$

$$[\mathbf{1E}]^- + e^- \rightarrow [\mathbf{1F}\cdots\mathbf{1F}]^{2-} \quad \text{Process 4}$$
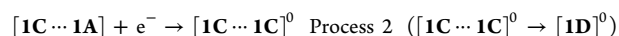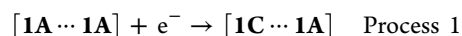

Figure 8. IR-SEC spectra of **1** (A) with $^{12}CO_2$ (black) and $^{13}CO_2$ (red) showing the results of sequential scans at potentials corresponding to the first reduction potential of **1** (−1.4 V vs Ag/Ag+ pseudo-RE). IR spectra (B) taken at resting potential after the application of catalytic potential, showing a mixture of the starting material **1** and the acetonitrile adduct (2020, 1913, and 1892 cm^{-1} and high-frequency stretch at 2037 cm^{-1}, respectively). Interestingly, the Re carbonyl bands observed after catalytic potentials under $^{13}CO_2$ atmosphere show the incorporation of ^{13}CO; the higher frequency bands assigned to the starting material and solvent species disappear almost entirely, replaced by bands at 1997 and 1977 cm^{-1}. Over time, IR stretches assigned to ^{12}CO (2137 cm^{-1}), ^{13}CO (2090 cm^{-1}), $^{12}CO_3^{2-}$ (1677 and 1648 cm^{-1}), and $^{13}CO_3^{2-}$ (1632 and 1594 cm^{-1}) grow with the concomitant consumption of substrate. GC/Ag/Pt IR-SEC cell; 3.6 mM (black), 3.5 mM (red) **1**, 0.1 M TBAPF$_6$/MeCN.

The fact that the first process is observed at all in CV suggests that formation of the neutral hydrogen-bonded dimer is quite fast and/or that its formation constant is >1 (K_a > 1). Using NMR concentration studies we estimate that the K_a for the neutral dimer of **1** ([**1A**⋯**1A**]) is 290 M^{-1} (Figure S13).[57] The second process also installs the Re−Re bond between the two metal centers, when CO_2 is not present. This was confirmed by IR-SEC and chemical reductions (Figures S14 and S15). This is also the potential at which catalysis occurs in the presence of CO_2 in MeCN. Based on the splitting between the first and second processes, we estimate the comproportionation constant, K_c, to be 340.[58] The third and fourth processes also show splitting caused by the persistence of hydrogen bonds. The third process corresponds to reduction, but not cleavage, of a hydrogen-bonded and Re−Re bonded dimer. The fourth process corresponds to reduction and cleavage of the dimer. The active state is therefore best described as a neutral hydrogen-bonded dimer with two five-coordinate Re^0 metal centers in close proximity, which is an intermediate to the formation of a Re−Re bond.

Appending simple amide groups to a well-characterized electrocatalyst dramatically influences the mechanism of CO_2 reduction. The methyl acetamidomethyl groups of complex **1** cause a hydrogen-bond-driven association of 2 equiv of the singly reduced complex, enhancing a bimolecular catalytic mechanism for the disproportionation of CO_2 to CO and CO_3^{2-}. This reaction has the merit of operating at a lower potential than the unimolecular mechanism (ca. 250 mV). Although the maximum TOF and Faradaic efficiency for CO are lower for this mechanism, further modifications might enable enhancement of these catalytic parameters too. The use of hydrogen bonding to drive assembly of catalytically advantageous structures is common in biological systems, but less so for synthetic molecular catalysts.[59−62] The use of hydrogen bonding and other driving forces for molecular assembly of abiotic catalysts promises to be a powerful way to alter catalytic mechanisms and potentially enhance catalyst properties, independent of more typical approaches that rely on unimolecular steric and electronic effects. The present results suggest new opportunities to optimize catalyst performance through the formation of supra- and macromolecular assemblies.

■ METHODS AND INSTRUMENTATION

General. ^{1}H NMR spectra were recorded on a 400 MHz Varian spectrometer at 298 K and referenced to solvent shifts. Data manipulations were completed using MestReNova and Jeol software. Infrared spectra were taken on a Thermo Scientific Nicolet 6700 or a Bruker Equinox 55 spectrometer. Microanalyses were performed by NuMega Resonance Laboratories, San Diego, CA for C, H, and N.

Solvents and Chemicals. All solvents were obtained from Fisher Scientific. Any dry solvents were dried in house by storing in a moisture free environment and dried on a custom drying system running through two alumina columns prior to use. All compounds were obtained from Fisher Scientific or Sigma-Aldrich and used as obtained unless otherwise specified. 4,4′-dicyano-2,2′-bipyridine was obtained from HetCat and used without further purification. Tetrabutylammonium hexafluorophosphate (TBAPF$_6$, Aldrich, 98%) was recrystallized from CH_3OH twice and dried at 90 °C overnight before use in electrochemical experiments.

Computational Methods. MD simulations were carried out with the Gromacs 4.6 software package[63] using explicit MeCN or *N,N*-DMF solvent at 298 K. All bonded and nonbonded parameters that do not involve a rhenium element were assigned from the general Amber force field.[64] Quantum methods (below) were used to optimize the

dimer structure and generate bonded parameters involving central rhenium atom. Nonbonded parameters for rhenium in the octahedral configuration were obtained from the universal force field.[65] Partial atomic charges were derived by fitting the electrostatic potential produced by quantum calculations using the restrained electrostatic potential approach.[66] Restraints were placed on the angles of O−C−Re to maintain the proper positions of the carbonyl groups.

Each dimer species was solvated in a cubic box with an edge length of ∼6 nm, energy-minimized using the steepest-descent algorithm and equilibrated for 1 ns at constant volume and temperature and then again at constant temperature and pressure. The subsequent production phase was run for at least 50 ns at constant temperature and pressure. Position restraints were applied to the solutes during the equilibration phases. The particle mesh Ewald method[67] was used for electrostatic interaction, and the cutoff distance of Lennard-Jones interactions was set as 10 Å.

Quantum calculations were carried out in the Gaussian 09 program[68] using the pure DFT functional M06-L[69] in conjunction with the conductor-like polarizable continuum model.[70] Restricted wave functions RM06-L were employed for closed shell systems, and unrestricted theory UM06-L was employed for open-shell systems. The 6-31++G(d,p) Pople basis set was selected for all the light atoms (H, C, N, O, and Cl), and the LANL2DZ (Los Alamos National Laboratory 2 double ζ) effective core potential as well as the corresponding basis set were used on the rhenium center. In preliminary tests on a series of rhenium bipyridyl compounds, this approach provided good agreement with experimental geometries, IR frequencies, and redox potentials (data not shown). The CO_2 bridged dimer was optimized in gas phase using a smaller basis set 6-31G* for the light atoms due to the high computational cost.

Synthetic Methods. Re(4,4′-dimethyl-2,2′-bipyridine)(CO)$_3$Cl (**2**) was prepared according to literature procedure.[8]

4,4′-Bis(aminomethyl)-2,2′-bipyridine.[40] A Parr hydrogenator flask was charged with a suspension of 4,4′-dicyano-2,2′-bipyridine (1.0 g, 4.8 mmol) and Pd/C (0.850 g) in a mixture of EtOH (150 mL), THF (60 mL), and concentrated HCl (37% aqueous, 2 mL). This suspension was heated at 50 °C under H$_2$ atmosphere (20 psi) for 48 h on a Parr hydrogenator. After being allowed to cool to room temperature, the flask was placed at −20 °C overnight before the acid salt of the product and Pd/C were removed from the suspension by vacuum filtration over Celite. The precipitated acid salt was dissolved in hot CH_3OH (200 mL, ∼ 50 °C) and filtered into a clean round-bottom flask. The resulting pink solution was condensed under reduced pressure to yield the acid salt of 4,4′-bis(aminomethyl)-2,2′-bipyridine as a pink powder. This powder was dissolved in minimal H$_2$O (∼5 mL) before NaOH (2.0 g) was added. This mixture was stirred vigorously (20 min) before being diluted by the addition of deionized H$_2$O (50 mL). This aqueous solution was extracted with CH_2Cl_2 (4 × 50 mL) and the combined organic layers were dried with anhydrous K$_2$CO$_3$ before being filtered and condensed under reduced pressure to reveal an off-white powder. Yield: 0.78 g, 75%. ^{1}H NMR (d_2-CD$_2$Cl$_2$, 400 MHz): δ 8.58 (sh d, 2H, Ar*H*), 8.40 (sh s, 2H, Ar*H*), 7.30 (sh d, 2H, Ar*H*), 3.96 (sh s, 4H, Ar*CH$_2$NH$_2$*), 1.52 (br s, 4H, Ar*CH$_2$NH$_2$*). ESI-MS (*m/z*) [M + H]$^+$: calcd: 215.1; found: 215.2. Elemental analysis for C$_{12}$H$_{14}$N$_4$ calcd: C 67.27, H 6.59, N 26.15; found: C 66.83, H 7.00, N 25.87.

4,4′-bis(methyl acetamidomethyl)-2,2′-bipyridine. A round-bottom flask was charged with 4,4′-bis(aminomethyl)-2,2′-bipyridine (0.300 g, 1.4 mmol) and triethylamine (0.41 mL, 2.9 mmol) in CH_2Cl_2 (250 mL). To this solution was slowly added acetic anhydride (0.28 mL, 2.9 mmol), and the resulting mixture was stirred overnight under N$_2$ atmosphere (∼16 h). The resulting white suspension was quenched with dilute Na$_2$CO$_3$ (aq, 50 mL) and extracted with ethyl acetate (3 × 100 mL) and CH_2Cl_2 (2 × 100 mL). The organic layers were combined and dried with Na$_2$SO$_4$ before being filtered and condensed under reduced pressure. If the reaction was incomplete, the dried product was loaded onto neutral alumina and purified chromatographically on a Combiflash silica column with a 0 to 10% CH_3OH in CHCl$_3$ gradient over 30 min. The eluent was monitored by UV−vis at 254 and 280 nm for the product. Yield: 0.21 g, 50%. ^{1}H

NMR (d_4-CD$_3$OD, 400 MHz): δ 8.58 (sh d, 2H, ArH), 8.23 (sh s, 2H, ArH), 7.36 (sh d, 2H, ArH), 4.49 (sh s, 4H, ArCH_2NHC(O)CH$_3$), 2.06 (s, 6H, CH$_2$NHC(O)CH_3). ESI-MS (m/z) [M + H]$^+$: calcd 299.2; found: 299.4. Elemental analysis for C$_{16}$H$_{18}$N$_4$O$_2$·(CH$_3$OH) calcd: C 61.80, H 6.71, N 16.96; found: C 62.11, H 8.12, N 17.08.

Re(4,4′-bis(methyl acetamidomethyl)-2,2′-bipyridine)(CO)$_3$Cl, 1. An oven-dried 250 mL round-bottom flask with a stir bar was charged with 4,4′-bis(acetoamidomethyl)-2,2′-bipyridine (0.300 g, 1 mmol), Re(CO)$_5$Cl (0.364 g, 1 mmol), and dry toluene (50 mL) under inert atmosphere (N$_2$). This flask was attached to a reflux condenser and heated to reflux for 3 h during which time the suspension turned from white to yellow. When the flask had cooled, solvent was removed under reduced pressure. The resulting yellow solid was recrystallized from CH$_3$OH/Et$_2$O at −20 °C to yield a yellow microcrystalline powder. Yield: 0.55 g, 91% ^{1}H NMR (d_3-CD$_3$CN, 400 MHz): δ 8.90 (sh d, 2H, ArH), 8.28 (sh s, 2H, ArH), 7.50 (sh d-d, 2H, ArH), 7.06 (br s, 2H, ArCH$_2$NHC(O)CH$_3$), 4.52 (d, 4H, ArCH_2NHC(O)CH$_3$), 2.01 (sh s, 6H, ArCH$_2$NHC(O)CH_3). ESI-MS (m/z) [M − Cl + CH$_3$OH]$^+$: calcd 601.1; found: 601.4. Elemental analysis for C$_{19}$H$_{18}$ClN$_4$O$_5$Re calcd: C 37.78, H 3.00, N 9.28; found: C 37.32, H 3.40, N 9.27.

Electrochemistry. Electrochemical experiments were carried out using a BAS Epsilon potentiostat. For all experiments, a single compartment cell was used with dry stir bar, and a dry needle was connected to control the atmosphere. A 3 mm diameter glassy carbon (GC) electrode from BASi was employed as the working electrode (WE). The counter electrode (CE) was a platinum (Pt) wire and the reference electrode (RE) was a silver/silver chloride (Ag/AgCl) electrode separated from solution by a Vycor tip. Experiments were run with and without an added internal reference of ferrocene. All solutions were in dry MeCN and contained 1 mM of catalyst and 0.1 M tetrabutylammonium hexafluorophosphate (TBAPF$_6$) as the supporting electrolyte and were interrogated at scan rates of 100 mV/s, unless otherwise noted. Experiments were purged with N$_2$ or CO$_2$ (to saturation at 0.28 M) before CVs were taken and stirred in between successive experiments. All experiments were reported referenced an internal ferrocene standard except for the bulk electrolysis experiments, which used the pseudo-RE Ag/AgCl behind a Vycor tip.

IR Spectroelectrochemistry. The experimental setup and design of the IR-SEC cell has been published previously by our lab.[41,45] A Pine Instrument Company model AFCBP1 bipotentiostat was employed. As the potential was scanned, thin-layer bulk electrolysis was monitored by Fourier transform reflectance IR off the electrode surface. All experiments were conducted in 0.1 M TBAPF$_6$/MeCN solutions with catalyst concentrations of ~5 mM (unless otherwise noted) prepared under a nitrogen atmosphere. For IR-SEC experiments under catalytic conditions, air-free samples were sparged briefly with ^{12}CO$_2$ or ^{13}CO$_2$ (10−20 s). The IR-SEC cells used ([WE]/[RE]/[CE]) were either GC/Ag/Pt or Pt/Ag/Pt, meaning that all potentials were in reference to a pseudo-RE, Ag/Ag+ (~+200 mV from the Fc/Fc+ couple).

X-ray Crystallography. Single-crystal X-ray diffraction studies reported herein were carried out on a Bruker Kappa APEX-II CCS diffractometer equipped with MoKα radiation (λ = 0.71073 Å). The crystals were mounted on a Cryoloop while in Paratone oil. The data was collected under a stream of N$_2$ gas at 100(2) K using ω and ϕ scans. Data were integrated using the Bruker SAINT software program and scaled using SADABS software. A complete phasing model consistent with the molecular structure was produced by SHELXS direct methods. Non-hydrogen atoms were reined anisotropically by full matrix least-squares (SHELXL-97).[71] All hydrogen atoms were determined using a riding model with positions constrained to their parent atom using the appropriate FHIX command. Crystallographic data is in Supporting Information (Tables S2 and S3).

■ ASSOCIATED CONTENT

⑤ Supporting Information

Additional information regarding species synthesized herein, including electrochemical responses, IR-SEC, movies of MD simulations, and crystallographic data. This material is available free of charge via the Internet at http://pubs.acs.org.

■ AUTHOR INFORMATION

Corresponding Authors
mgilson@ucsd.edu
ckubiak@ucsd.edu

Notes
The authors declare no competing financial interest. M.K.G. has an equity interest in, and is a cofounder and scientific advisor of VeraChem LLC.

■ ACKNOWLEDGMENTS

■ REFERENCES

(1) Benson, E. E.; Kubiak, C. P.; Sathrum, A. J.; Smieja, J. M. *Chem. Soc. Rev.* **2009**, *38*, 89.

(2) Finn, C.; Schnittger, S.; Yellowlees, L. J.; Love, J. B. *Chem. Commun.* **2012**, *48*, 1392.

(3) Inglis, J. L.; MacLean, B. J.; Pryce, M. T.; Vos, J. G. *Coord. Chem. Rev.* **2012**, *256*, 2571.

(4) Costentin, C.; Robert, M.; Saveant, J.-M. *Chem. Soc. Rev.* **2013**, *42*, 2423.

(5) Qiao, J.; Liu, Y.; Hong, F.; Zhang, J. *Chem. Soc. Rev.* **2014**, *43*, 631.

(6) Appel, A. M.; Bercaw, J. E.; Bocarsly, A. B.; Dobbek, H.; DuBois, D. L.; Dupuis, M.; Ferry, J. G.; Fujita, E.; Hille, R.; Kenis, P. J. A.; Kerfeld, C. A.; Morris, R. H.; Peden, C. H. F.; Portis, A. R.; Ragsdale, S. W.; Rauchfuss, T. B.; Reek, J. N. H.; Seefeldt, L. C.; Thauer, R. K.; Waldrop, G. L. *Chem. Rev.* **2013**, *113*, 6621.

(7) Hawecker, J.; Lehn, J.-M.; Ziessel, R. *J. Chem. Soc., Chem. Comm.* **1984**, 328.

(8) Smieja, J. M.; Kubiak, C. P. *Inorg. Chem.* **2010**, *49*, 9283.

(9) Hawecker, J.; Lehn, J.-M.; Ziessel, R. *Helv. Chim. Acta* **1986**, *69*, 1990.

(10) Smieja, J. M.; Benson, E. E.; Kumar, B.; Grice, K. A.; Seu, C. S.; Miller, A. J. M.; Mayer, J. M.; Kubiak, C. P. *Proc. Natl. Acad. Sci. U.S.A.* **2012**, *109*, 15646.

(11) Morris, A. J.; Meyer, G. J.; Fujita, E. *Acc. Chem. Res.* **2009**, *42*, 1983.

(12) Parkin, A.; Seravalli, J.; Vincent, K. A.; Ragsdale, S. W.; Armstrong, F. A. *J. Am. Chem. Soc.* **2007**, *129*, 10328.

(13) Jormakka, M.; Törnroth, S.; Byrne, B.; Iwata, S. *Science* **2002**, *295*, 1863.

(14) Boyington, J. C.; Gladyshev, V. N.; Khangulov, S. V.; Stadtman, T. C.; Sun, P. D. *Science* **1997**, *275*, 1305.

(15) Reda, T.; Plugge, C. M.; Abram, N. J.; Hirst, J. *Proc. Natl. Acad. Sci. U.S.A.* **2008**, *105*, 10654.

(16) Can, M.; Armstrong, F. A.; Ragsdale, S. W. *Chem. Rev.* **2014**, *114*, 4149.

(17) Krokan, H. E.; Standal, R.; Slupphaug, G. *Biochem. J.* **1997**, *325*, 1.

(18) Pickart, C. M.; Eddins, M. J. *Biochim. Biophys. Acta, Mol. Cell Res.* **2004**, *1695*, 55.

(19) Nordlund, P.; Reichard, P. *Annu. Rev. Biochem.* **2006**, *75*, 681.

(20) Helm, M. L.; Stewart, M. P.; Bullock, R. M.; DuBois, M. R.; DuBois, D. L. *Science* **2011**, *333*, 863.

(21) Rakowski DuBois, M.; DuBois, D. L. *Chem. Soc. Rev.* **2009**, *38*, 62.

(22) Gloaguen, F.; Rauchfuss, T. B. *Chem. Soc. Rev.* **2009**, *38*, 100.

(23) Ginovska-Pangovska, B.; Dutta, A.; Reback, M. L.; Linehan, J. C.; Shaw, W. J. *Acc. Chem. Res.* **2014**, *47*, 2621.

(24) Costentin, C.; Drouet, S.; Robert, M.; Savéant, J.-M. *Science* **2012**, *338*, 90.

(25) Hammes, G. G. *Biochemistry* **2002**, *41*, 8221.

(26) Raushel, F. M.; Thoden, J. B.; Holden, H. M. *Acc. Chem. Res.* **2003**, *36*, 539.

(27) Williams, D. H.; Stephens, E.; O'Brien, D. P.; Zhou, M. *Angew. Chem., Int. Ed.* **2004**, *43*, 6596.

(28) Benson, E. E.; Kubiak, C. P. *Chem. Commun.* **2012**, *48*, 7374.

(29) Benson, E. E.; Grice, K. A.; Smieja, J. M.; Kubiak, C. P. *Polyhedron* **2013**, *58*, 229.

(30) Benson, E. E.; Sampson, M. D.; Grice, K. A.; Smieja, J. M.; Froehlich, J. D.; Friebel, D.; Keith, J. A.; Carter, E. A.; Nilsson, A.; Kubiak, C. P. *Angew. Chem., Int. Ed.* **2013**, *52*, 4841.

(31) Grice, K. A.; Gu, N. X.; Sampson, M. D.; Kubiak, C. P. *Dalton Trans.* **2013**, *42*, 8498.

(32) Keith, J. A.; Grice, K. A.; Kubiak, C. P.; Carter, E. A. *J. Am. Chem. Soc.* **2013**, *135*, 15823.

(33) Sampson, M. D.; Froehlich, J. D.; Smieja, J. M.; Benson, E. E.; Sharp, I. D.; Kubiak, C. P. *Energy Environ. Sci.* **2013**, *6*, 3748.

(34) Sullivan, B. P.; Bolinger, C. M.; Conrad, D.; Vining, W. J.; Meyer, T. J. *J. Chem. Soc., Chem. Comm.* **1985**, 1414.

(35) Hayashi, Y.; Kita, S.; Brunschwig, B. S.; Fujita, E. *J. Am. Chem. Soc.* **2003**, *125*, 11976.

(36) Agarwal, J.; Fujita, E.; Schaefer, H. F.; Muckerman, J. T. *J. Am. Chem. Soc.* **2012**, *134*, 5180.

(37) Dempsey, J. L.; Brunschwig, B. S.; Winkler, J. R.; Gray, H. B. *Acc. Chem. Res.* **2009**, *42*, 1995.

(38) Muckerman, J. T.; Fujita, E. *Chem. Commun.* **2011**, *47*, 12456.

(39) McKone, J. R.; Marinescu, S. C.; Brunschwig, B. S.; Winkler, J. R.; Gray, H. B. *Chem. Sci.* **2014**, *5*, 865.

(40) Beer, P. D.; Szemes, F.; Passaniti, P.; Maestri, M. *Inorg. Chem.* **2004**, *43*, 3965.

(41) Machan, C. W.; Sampson, M. D.; Chabolla, S. A.; Dang, T.; Kubiak, C. P. *Organometallics* **2014**, *33*, 4550.

(42) *CRC Handbook of Chemistry and Physics*, 95th ed. 2014.

(43) Christensen, P.; Hamnett, A.; Muir, A. V. G.; Timney, J. A. *J. Chem. Soc., Dalton Trans.* **1992**, 1455.

(44) Stor, G. J.; Hartl, F.; van Outersterp, J. W. M.; Stufkens, D. J. *Organometallics* **1995**, *14*, 1115.

(45) Zavarine, I. S.; Kubiak, C. P. *J. Electroanal. Chem.* **2001**, *495*, 106.

(46) *Spectroelectrochemistry*; Royal Society of Chemistry: Cambridge, England, 2008.

(47) Kaim, W.; Fiedler, J. *Chem. Soc. Rev.* **2009**, *38*, 3373.

(48) Torii, H.; Tatsumi, T.; Kanazawa, T.; Tasumi, M. *J. Phys. Chem. B* **1998**, *102*, 309.

(49) Barth, A.; Zscherp, C. *Q. Rev. Biophys.* **2002**, *35*, 369.

(50) Fujita, E.; Muckerman, J. T. *Inorg. Chem.* **2004**, *43*, 7636.

(51) Breikss, A. I.; Abruna, H. D. *J. Electroanal. Chem.* **1986**, *201*, 347.

(52) Cosnier, S.; Deronzier, A.; Moutet, J.-C. *New J. Chem.* **1990**, *14*, 831.

(53) Savéant, J. M.; Vianello, E. *Electrochim. Acta* **1963**, *8*, 905.

(54) Bard, A. J.; Faulkner, L. R. *Electrochemical Methods: Fundamentals and Applications*, 2nd ed.; John Wiley & Sons, Inc.: Hoboken, NJ, 2001.

(55) Sampson, M. D.; Nguyen, A. D.; Grice, K. A.; Moore, C. E.; Rheingold, A. L.; Kubiak, C. P. *J. Am. Chem. Soc.* **2014**, *136*, 5460.

(56) Simón-Manso, E.; Kubiak, C. P. *Organometallics* **2004**, *24*, 96.

(57) Lafitte, V. G. H.; Aliev, A. E.; Horton, P. N.; Hursthouse, M. B.; Bala, K.; Golding, P.; Hailes, H. C. *J. Am. Chem. Soc.* **2006**, *128*, 6544.

(58) Ito, T.; Hamaguchi, T.; Nagino, H.; Yamaguchi, T.; Kido, H.; Zavarine, I. S.; Richmond, T.; Washington, J.; Kubiak, C. P. *J. Am. Chem. Soc.* **1999**, *121*, 4625.

(59) Perálvarez-Marín, A.; Lórenz-Fonfría, V. A.; Bourdelande, J.-L.; Querol, E.; Kandori, H.; Padrós, E. *J. Mol. Biol.* **2007**, *368*, 666.

(60) de Rege, P.; Williams, S.; Therien, M. *Science* **1995**, *269*, 1409.

(61) Reece, S. Y.; Hodgkiss, J. M.; Stubbe, J.; Nocera, D. G. *Philos. Trans. R. Soc., B* **2006**, *361*, 1351.

(62) Sigala, P. A.; Tsuchida, M. A.; Herschlag, D. *Proc. Natl. Acad. Sci. U.S.A.* **2009**, *106*, 9232.

(63) Pronk, S.; Pall, S.; Schulz, R.; Larrson, P.; Bjelkmar, P.; Apostolov, R.; Shirts, M. R.; Smith, J. C.; Kasson, P. M.; van der Spoel, D.; Hess, B.; Lindahl, E. *Bioinformatics* **2013**, *29*, 845.

(64) Wang, J. M.; Wolf, R. M.; Caldwell, J. W.; Kollman, P. A.; Case, D. A. *J. Comput. Chem.* **2004**, *25*, 1157.

(65) Rappe, A. K.; Casewit, C. J.; Colwell, K. S.; Goddard, W. A., III; Skiff, W. M. *J. Am. Chem. Soc.* **1992**, *114*, 10024.

(66) Bayly, C. I.; Cieplak, P.; Cornell, W.; Kollman, P. A. *J. Phys. Chem.* **1993**, *97*, 10269.

(67) Essman, U.; Perera, L.; Berkowitz, M. L.; Darden, T.; Lee, H.; Pedersen, L. G. *J. Chem. Phys.* **1995**, *103*, 8577.

(68) Frisch, M. J.; Trucks, G. W.; Schlegel, H. B.; Scuseria, G. E.; Robb, M. A.; Cheeseman, J. R.; Scalmani, G.; Barone, V.; Mennucci, B.; Petersson, G. A.; Nakatsuji, H.; Caricato, M.; Li, X.; Hratchian, H. P.; Izmaylov, A. F.; Bloino, J.; Zheng, G.; Sonnenberg, J. L.; Hada, M.; Ehara, M.; Toyota, K.; Fukuda, R.; Hasegawa, J.; Ishida, M.; Nakajima, T.; Honda, Y.; Kitao, O.; Nakai, H.; Vreven, T.; Montgomery, J. A., Jr.; Peralta, J. E.; Ogliaro, F.; Bearpark, M.; Heyd, J. J.; Brothers, E.; Kudin, K. N.; Staroverov, V. N.; Kobayashi, R.; Normand, J.; Raghavachari, K.; Rendell, A.; Burant, J. C.; Iyengar, S. S.; Tomasi, J.; Cossi, M.; Rega, N.; Millam, J. M.; Klene, M.; Knox, J. E.; Cross, J. B.; Bakken, V.; Adamo, C.; Jaramillo, J.; Gomperts, R.; Stratmann, R. E.; Yazyev, O.; Austin, A. J.; Cammi, R.; Pomelli, C.; Ochterski, J. W.; Martin, R. L.; Morokuma, K.; Zakrzewski, V. G.; Voth, G. A.; Salvador, P.; Dannenberg, J. J.; Dapprich, S.; Daniels, A. D.; Farkas, O.; Foresman, J. B.; Ortiz, J. V.; Cioslowski, J.; Fox, D. J. *Gaussian 09*; Gaussian, Inc.: Wallingford, CT, 2009.

(69) Zhao, Y.; Truhlar, D. G. *J. Chem. Phys.* **2006**, *125*, 194101.

(70) Barone, V.; Cossi, M. *J. Phys. Chem. A* **1998**, *102*, 1995.

(71) Sheldrick, G. *Acta Crystallogr., Sect. A* **2008**, *64*, 112.